Constant bond breakup probability model for reversible aggregation processes

G. Odriozola,[1] A. Schmitt,[2] A. Moncho-Jordá,[2] J. Callejas-Fernández,[2] R. Martínez-García,[2] R. Leone,[1] and R. Hidalgo-Alvarez[2,*]

[1]*Departamento de Química Física y Matemática, Facultad de Química, Universidad de la República, 11800 Montevideo, Uruguay*

[2]*Departamento de Física Aplicada, Universidad de Granada, Campus de Fuentenueva, E-18071 Granada, Spain*

(Received 21 June 2001; revised manuscript received 19 September 2001; published 21 February 2002)

Reversible aggregation processes were simulated for systems of freely diffusing sticky particles. Reversibility was introduced by allowing that all bonds in the system may break with a given probability per time interval. In order to describe the kinetics of such aggregation-fragmentation processes, a fragmentation kernel was developed and then used together with the Brownian aggregation kernel for solving the corresponding kinetic master equation. The deduced fragmentation kernel considers a single characteristic lifetime for all bonds and accounts for the cluster morphology by averaging over all possible configurations for clusters of a given size. It became evident that the simulated cluster-size distributions could be described only when an additional fragmentation effectiveness was considered. Doing so, the stochastic solutions were in good agreement with the simulated data.

DOI: 10.1103/PhysRevE.65.031405 PACS number(s): 82.70.Dd, 82.40.Bj, 02.50.−r

I. INTRODUCTION

Reversible aggregation processes are usually considered as the result of two competing effects, particle aggregation and cluster fragmentation. Aggregation processes are of fundamental importance in a wide variety of natural systems and industrial applications such as aerosol and soot particle growth, droplet formation, and the production of polymers, paints, and biological material among others [1–3]. Fragmentation phenomena may be observed in processes such as droplet degradation and cluster breakup [4–6]. In many cases, however, both phenomena may occur simultaneously [7–9].

In this paper, we study reversible aggregation processes of initially monodisperse systems by means of computer simulations. For this purpose, the clusters were considered to move due to free Brownian motion and to form a new bond as soon as they collide. In order to introduce reversibility, all bonds in the system were allowed to break with a given probability per time step. For simplicity, we assumed the breakup probability to be the same for all bonds. This situation corresponds to a system where the particle interaction potential shows a pronounced but finite minimum at very short distances. At initial stages, cluster breakup cannot occur since no bonds exist in the system and the cluster-size distribution evolves in a way similar to the irreversible diffusion limited cluster-cluster aggregation (DLCA) regime. After sufficiently long time, however, cluster breakup becomes important and, at very long times, the system reaches a dynamic equilibrium between aggregation and fragmentation. In order to describe the kinetics of such processes, a stochastic master equation approach was used to calculate the time evolution of the cluster-size distribution. For this purpose, an aggregation-fragmentation kernel had to be developed. This was achieved by combining the Brownian kernel, which is known to model pure DLCA, with a novel fragmentation kernel.

The paper is organized as follows: Section I is the Introduction. Section II reviews the theoretical background needed for describing the kinetics of reversible aggregation processes. In Sec. III, the fragmentation kernel is deduced. Section IV tackles the results and a discussion thereof. Finally, Sec. V summarizes the results and extracts the conclusions.

II. THEORETICAL BACKGROUND

The stochastic formulation for describing the kinetics of a reactive system is given by the master equation [10]. The master equations for irreversible aggregation and pure fragmentation processes may be found in Refs. [6,11,12]. In this paper, we combine both cases in order to describe reversible aggregation processes.

If $P(\vec{N},t)$ denotes the probability for finding the system in the state $\vec{N}=(N_1,N_2,\ldots,N_n)$ at time t, its time evolution is determined by

$$\begin{aligned}\frac{dP(\vec{N},t)}{dt}=&\frac{1}{2V}\sum_{i}^{\infty}\sum_{j}^{\infty}k_{ij}[(N_i+1)(N_j+1+\delta_{ij})P(\vec{N}_{ij}^{+},t)\\&-N_i(N_j-\delta_{ij})P(\vec{N},t)]\\&+\frac{1}{2V}\sum_{n=2}^{\infty}\left[(N_n+1)\sum_{i=1}^{n-1}f_{i(n-i)}P(\vec{N}_{i(n-i)}^{-},t)\right.\\&\left.-N_n\sum_{i=1}^{n-1}f_{i(n-i)}P(\vec{N},t)\right],\end{aligned}\tag{1}$$

where N_i is the number of i-size particles, k_{ij} is the aggregation kernel, f_{ij} is the fragmentation kernel, and δ_{ij} is the Kronecker function. The displaced states N_{ij}^{+} and N_{ij}^{-} are given by

*Author to whom correspondence should be addressed. Email address: rhidalgo@ugr.es

$$\vec{N}_{ij}^{+}=\begin{cases}(\ldots,N_i+1,\ldots,N_j+1,\ldots,N_{i+j}-1,\ldots) & \text{for } i\neq j\\ (\ldots,N_i+2,\ldots,N_{2i}-1,\ldots) & \text{for } i=j,\end{cases}$$

$$\vec{N}_{ij}^{-}=\begin{cases}(\ldots,N_i-1,\ldots,N_j-1,\ldots,N_{i+j}+1,\ldots) & \text{for } i\neq j\\ (\ldots,N_i-2,\ldots,N_{2i}+1,\ldots) & \text{for } i=j.\end{cases}$$

The aggregation kernel k_{ij} represents the average rate constant under which an *i*-size cluster reacts with a *j*-size cluster and forms an $(i+j)$-size aggregate. The fragmentation kernel f_{ij} denotes the mean rate constant at which $(i+j)$-size cluster break spontaneously into two *i*- and *j*-size fragments. Both, the aggregation and the fragmentation kernel, have to be understood as orientational and configurational averages. They contain all physical information about the aggregation-fragmentation mechanism.

A classification scheme for homogeneous aggregation kernels was introduced by van Dongen and Ernst [13]. They defined two scaling exponents λ and μ according to the relationship

$$k_{(ai)(aj)}\sim a^{\lambda}k_{ij},$$

$$k_{i\ll j}\sim i^{\mu}j^{\lambda-\mu}, \tag{2}$$

where $a>1$ is a constant. Since the cluster reactivity cannot rise faster than its mass, kernels with either $\lambda>2$ or $(\lambda-\mu)>1$ are nonphysical for irreversible aggregation. The homogeneity parameter λ links the aggregation rate constants of two smaller clusters to the aggregation rate constants of two larger ones. For pure irreversible aggregation, kernels with $\lambda\leqslant 1$ show a nongelling behavior, i.e., a cluster of infinite size is formed at infinite time. For $\lambda>1$, the rate of aggregation becomes so fast that an infinite size cluster forms at finite time (gel point). The exponent μ controls the rate at which big clusters bind to small clusters. For kernels with $\mu<0$, the big cluster small cluster union is favored.

Analogously, a similar classification scheme for fragmentation kernels may be proposed,

$$f_{(ai)(aj)}\sim a^{\lambda_f}f_{ij},$$

$$f_{i\ll j}\sim i^{\mu_f}j^{\lambda_f-\mu_f}, \tag{3}$$

where λ_f and μ_f are the scaling exponents for cluster fragmentation. Hence, λ_f links the fragmentation rate constants of smaller clusters to the fragmentation rate constants of larger ones. The exponent μ_f correlates the rates at which clusters break into similar or dissimilar fragments. Nonshattering fragmentation processes are characterized by $\lambda_f\geqslant -1$ [14,15]. For kernels with $\mu_f<0$, dissimilar breakup is favored.

The total fragmentation rate constant for clusters of size *n* is given by $F(n)=\frac{1}{2}\Sigma_{i+j=n}f_{ij}$. Assuming that $F(n)\sim n^x$, shattering fragmentation may be distinguished from nonshattering fragmentation by $x<0$ and $x>0$, respectively [6,16]. The irreversible DLCA regime is usually modeled using the Brownian kernel. This kernel was derived by considering solid spheres that approach due to Brownian motion and stick as soon as they come into physical contact. For fractal aggregates, its analytical form is given by

$$k_{ij}^{Brown}=\frac{1}{4}k_{11}^{Smol}(i^{(1/d_f)}+j^{(1/d_f)})(i^{(-1/d_f)}+j^{(-1/d_f)}), \tag{4}$$

where $k_{11}^{Smol}=8k_BT/3\eta$ is the dimer formation rate constant, d_f is the cluster fractal dimension, k_BT is the thermal energy, and η is the solvent viscosity [17,18]. This kernel has, according to Eq. (2), $\lambda=0$ and $\mu=-1/d_f$. Since we limit our simulations to aggregation-fragmentation processes of sticky particles, this kernel will be used as aggregation kernel k_{ij} in Eq. (1). The employed fragmentation kernel f_{ij} will be deduced in the following section.

III. DEVELOPING A FRAGMENTATION KERNEL

The fragmentation kernels most frequently found in the literature are the constant kernel $f_{ij}=f_{11}$, which has only one free parameter, and the sum fragmentation kernel, $f_{ij}=f_{11}(i+j)^{\alpha}$, which has two of them. These kernels are widely used since they are the simplest possible mathematical expressions for symmetric kernels [7,19–21]. Although they yield a reasonably good description of fragmentation kinetics, they are not based on sound physical grounds and so, we consider it necessary to develop a fragmentation kernel based on reasonable physical assumptions.

For this purpose, we assume all bonds to be of identical nature and define P_r as the probability for a bond to break during the time interval Δt. Considering a population of N_2 dimers, the change of N_2 due to fragmentation during the following time interval Δt is given by

$$\Delta N_2=-P_rN_2. \tag{5}$$

For very short time intervals, P_r should be proportional to Δt and so, we may write $P_r=\Delta t/\tau$, where τ is the average bond lifetime. Taking the limit $\Delta t\to 0$ in Eq. (5), one obtains the continuous differential equation

$$\frac{dN_2}{dt}=-\frac{N_2}{\tau}. \tag{6}$$

This equation is valid only for dimers, i.e., clusters that contain only one bond. In order to apply it to larger aggregates, it is necessary to consider all possible fragment sizes *i* and *j*

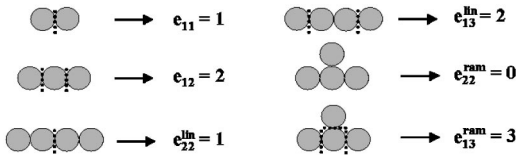

FIG. 1. Fragmentation possibilities and corresponding e_{ij} values for clusters smaller than pentamers.

to which the breakup of a given $n=(i+j)$-size cluster may lead. We indicate these possibilities using the subindices i and j

$$\left.\frac{dN_n}{dt}\right|_{ij} = -e_{ij}\frac{N_n}{\tau}. \tag{7}$$

Hence, the expression $dN_n/dt|_{ij}$ gives the fragmentation rate of n-size clusters due to breakup into i- and j-size fragments. The factor e_{ij} is the number of bonds contained in n size clusters which, on breakup, lead to i- and j-size fragments. For the sake of clarity, Fig. 1 schematizes the different fragmentation possibilities for dimers, trimers, and tetramers. The corresponding e_{ij} values are also indicated in the scheme. Dimers can break only into monomers and so, have $e_{11}=1$. Trimers, however, may fragment by breaking one of two bonds and consequently, have $e_{12}=2$. The situation becomes more complicated for larger clusters since they may have different configurations. In fact, the number of possible configurations is expected to increase with cluster size. For example, tetramers are either linear or branched (see Fig. 1). The former type of tetramers is characterized by $e_{13}^{lin}=2$ and $e_{22}^{lin}=1$ while branched tetramers have $e_{13}^{ram}=3$ and $e_{22}^{ram}=0$. For an aggregating system, both kinds of tetramers are formed and hence, it is convenient to average the e_{ij} values over all possible cluster structures. This implies that, for tetramers, the average e_{ij} should lie in the range of $2\leqslant e_{13}\leqslant 3$ and $0\leqslant e_{22}\leqslant 1$. Although it was not explicitly mentioned before, it can be clearly seen from Eq. (7) that the fragmentation kernel is given by

$$f_{ij}=\frac{e_{ij}(1+\delta_{ij})}{\tau}, \tag{8}$$

where δ_{ij} appears for the sake of consistency with Eq. (1). In order to obtain an analytical expression for e_{ij}, we analyze the fragmentation possibilities of simulated clusters. Therefore, off-lattice simulations were carried out for spherical particles of radius a inside a cubic box of side length L considering periodical boundary conditions (for further details, see Ref. [22]). The simulation conditions were the same as those detailed in Ref. [11], i.e., monomeric initial conditions, a total particle number $N_0=10^4$ and a step length $l_0=0.5a$. The box size was set to $L=437.6a$ in order to establish a volume fraction of 5.0×10^{-4}. Additionally, the possibility of bond breakup was introduced. For this purpose, a random number ξ uniformly distributed in $[0,1]$ is generated and compared with P_r for all bonds and at each time step. Only when $\xi<P_r$, the corresponding bond is broken and the fragments are separated a fixed distance $l_s=l_0/5$ in the direction of the line that connects the center of the particles involved in the bond breakup. If this movement leads to cluster overlapping, the fragments are joined again in a new bond. This implies that reversible aggregation allows for cluster rearrangement [23].

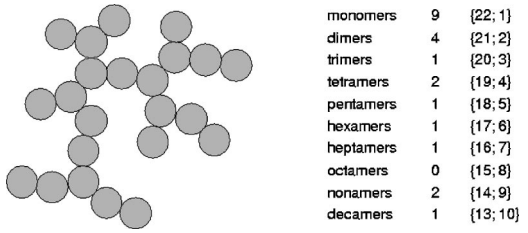

FIG. 2. Schematic diagram of a cluster of size $n=23$ (for the sake of simplicity represented only in two dimensions). The list shows the number of i-size fragments that may be obtained by breaking only one bond. The corresponding subindices for the e_{ij} matrix are indicated as $\{i;j\}$.

The obtained clusters were then analyzed one by one as schematized in Fig. 2. The analyzing procedure consists in counting the number of i-mers that may be generated by breaking only one bond of the selected cluster. This number is then averaged with those obtained for other clusters of the same size. By definition, this average is e_{ij}. In order to obtain good statistics, 10^5 individual clusters were considered within the cluster-size range of $[1,100]$. This means that the e_{ij} function could be accessed for i and $j\leqslant 50$. The calculated e_{ij} matrix is shown as a three-dimensional plot in Fig. 3(a). As expected, $e_{11}=1$ and $e_{12}=2$ were obtained. Furthermore, the values of $e_{13}=2.16$ and $e_{22}=0.845$ suggest that, at least for our simulations, linear tetramers are more frequently found than ramified ones.

In order to extrapolate the fragmentation kernel f_{ij} for clusters larger than 100-mers, the following empirical function was fitted to the assessed $e_{ij}(1+\delta_{ij})$ matrix,

$$e_{ij}(1+\delta_{ij})|_{fit}=p_1(i^{p_2}+j^{p_2})(i^{p_3}+j^{p_3})(ij)^{p_4}. \tag{9}$$

The fitted values were $p_1=0.4391$, $p_2=1.006$, $p_3=-1.007$, and $p_4=-0.1363$. For the smallest aggregates, it is convenient to assign the exactly known values $2e_{11}=e_{12}=2$. The fitted function is plotted in Fig. 3(b). The residuals r_{ij} defined as

$$r_{ij}=\frac{e_{ij}(1+\delta_{ij})-e_{ij}(1+\delta_{ij})|_{fit}}{e_{ij}(1+\delta_{ij})|_{fit}} \tag{10}$$

are shown in Fig. 3(c). As can be seen, the residuals seem to be randomly distributed around zero.

Since the aggregates produced by the simulations are loopless, there are $(n-1)$ bonds in every cluster containing n particles. This implies that $\Sigma_{i+j=n}e_{ij}(1+\delta_{ij})=2(n-1)$. Hence, a convenient way to estimate the accuracy of the fitted $e_{ij}(1+\delta_{ij})$ matrix consists in calculating the relative deviation of the sum term from its theoretical value $2(n-1)$. We found that the average misfit for the simulated aggregates ($n<100$) is about 0.8%. If one considers also the extrapolated values for larger aggregates, the average relative

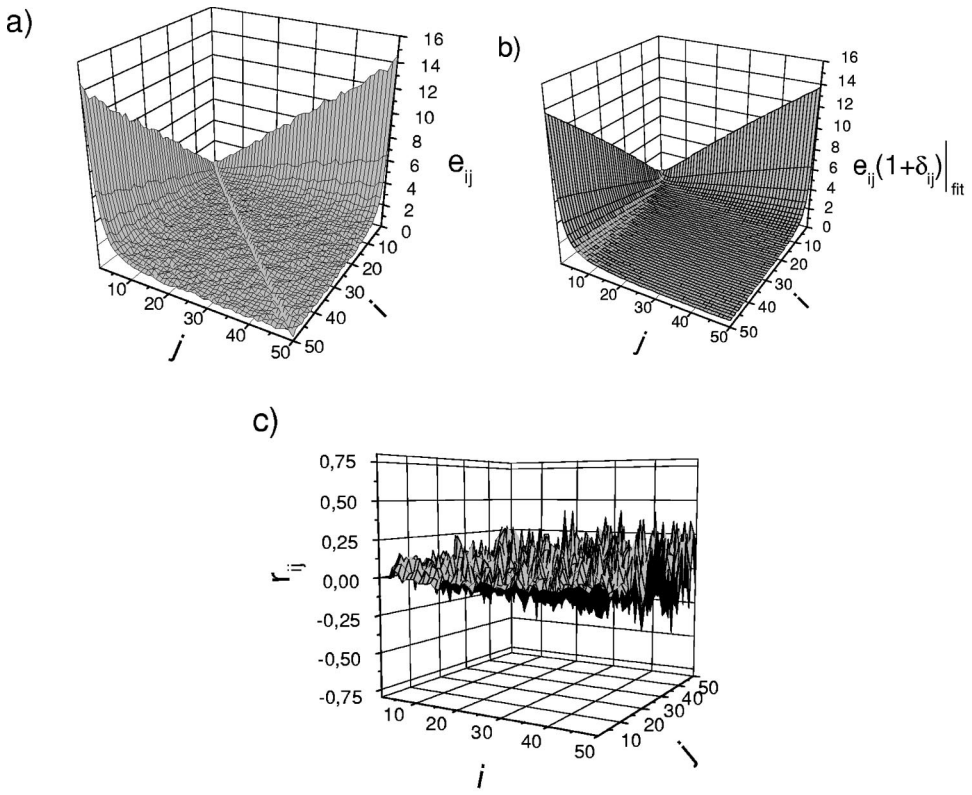

FIG. 3. Three-dimensional plots of (a) the e_{ij} matrix obtained from simulated clusters, (b) the fitted analytical function $e_{ij}(1+\delta_{ij})|_{fit}$, and (c) the corresponding residuals r_{ij} defined by Eqs. (9) and (10), respectively.

deviation becomes 1.1% and 3.1% for $n<200$ and $n<500$, respectively. This means that the fitted fragmentation kernel may be considered as a reasonably good approximation even though one should remind that the relative deviation from its correct form tends to increase for increasing aggregate size.

It should be noted that the diagonal elements of the e_{ij} matrix are always smaller than the off-diagonal elements (see Fig. 3). Hence, cluster breakup into fragments of similar size is less likely than cluster breakup into fragments of dissimilar size. This fact may easily be understood for the case of linear tetramers that have $e_{13}=2e_{22}$ (see Fig. 1). It is a particular case of the more general result that even-size linear clusters have always $e_{i\neq j}=2e_{i=j}$.

Resuming, we may affirm that the assumption of a bond independent breakup probability leads to a fragmentation kernel characterized by $\mu_f=-1.143$, i.e., a model where the clusters are more frequently broken into fragments of very dissimilar mass, and $\lambda_f=-0.273$, which indicates a slight decrease of the fragmentation kernel f_{ij} for increasing cluster size. This, of course, does not mean that larger clusters break less frequently than smaller ones. On the contrary, here, one obtains $F(n)=\frac{1}{2}\Sigma_{i+j=n}f_{ij}\sim n$, which corresponds clearly to a nonshattering regime.

IV. RESULTS

Equations (8) and (9) give a fitted analytical expression for the fragmentation kernel. In order to check its validity, we confront the time evolution of the cluster-size distribution obtained directly from simulations with the corresponding solutions of the reversible master equation. The simulations were performed for $P_r=0$ (DLCA), 1×10^{-5}, 2×10^{-5}, 3×10^{-5}, 4×10^{-5}, and 5×10^{-5}. The simulation time step was converted into real time using the relationship $\Delta t=l_0^2/6D_1$. Here, D_1 is the monomer diffusion coefficient that was assessed using Stokes's law. For aqueous systems of spherical particles of radius $a=3.15\times10^{-7}$ m at 293 K, $\Delta t=0.005\,897$ s was obtained. Consequently, the characteristic bond lifetimes for the above mentioned P_r values are $\tau=\infty$, 589.7 s, 294.8 s, 196.6 s, 147.4 s, and 117.9 s, respectively.

For solving the reversible master equation, both, the fragmentation and the aggregation kernels are needed. Since the simulations were carried out considering that all cluster-cluster collisions lead to bond formation, the Brownian aggregation kernel is employed together with Eqs. (8) and (9) as fragmentation kernel. The corresponding stochastic master equation was solved for 10^5 particles using the method described in Ref. [10]. The Brownian kernel depends on the dimer formation rate constant k_{11}^{Smol} and the fractal dimension d_f. The former parameter is given by $k_{11}^{Smol}=8k_BT/3\eta$, which yields 11.1×10^{-18} $m^3\,s^{-1}$ for aqueous systems at 293 K. The latter was directly assessed from the generated cluster structure by means of the radius of gyration method described in Ref. [24]. The fragmentation kernel depends only on τ and e_{ij}. Since the e_{ij} function is already known from Eq. (9) and τ is an input parameter for the simulations, the aggregation-fragmentation kernel is completely determined and there are no freely adjustable parameters left for fitting.

The obtained fractal dimensions are summarized in Table I. It can be observed that the cluster fractal dimension increases with increasing breakup probability until it reaches values close to approximately 2.0. Then, it seems to become

TABLE I. Average bond lifetime τ, cluster fractal dimension d_f, time necessary for reaching equilibrium t^{eq}, and weight average equilibrium cluster size n_w^{eq}, for the different bond breakup probabilities P_r.

P_r (10^5)	τ (s)	d_f	t^{eq} (s)	n_w^{eq}
0	∞	1.72 ± 0.04	∞	∞
1	598.7	1.83 ± 0.05	7000 ± 2000	100 ± 25
2	294.8	1.89 ± 0.04	3500 ± 1000	60 ± 15
3	196.6	2.06 ± 0.06	2500 ± 800	40 ± 10
4	147.4	1.97 ± 0.05	2000 ± 600	30 ± 8
5	117.9	1.99 ± 0.06	1800 ± 500	30 ± 5

constant and independent of the bond lifetime. This result is in good agreement with the value of 2.03 ± 0.05 reported by Kolb for lattice aggregation simulations with random bond breaking [25]. Furthermore, it has been proven that this model reaches an equilibrium state identical with the one obtained for branched polymers (lattice animals) [26,27].

Figure 4(a) shows the time evolution of the cluster-size distribution for $P_r=1\times10^{-5}$. Here, the symbols represent the simulated data while the solid lines indicate the corresponding master equation solution. At early stages, the system evolves very similar to those aggregating under irreversible DLCA conditions. This is not surprising since at the beginning only a few recently formed bonds exist in the system. Taking into account that their characteristic lifetime is approximately 600 s, it becomes evident that breakup effects cannot yet be important. At later stages, however, the number of monomers tends to stabilize and fluctuate around a constant value. The same behavior is also observed for the larger aggregates at longer times. The time evolution of the weight average cluster size n_w is shown in Fig. 4(b). As can be seen, it evolves in a similar manner. After a short initial transition period, a linear increase in time is observed as long as fragmentation effects are still negligible. When the system reaches a certain degree of aggregation, the growth rate decreases and finally, when the overall fragmentation rate equals the overall aggregation rate, a dynamic equilibrium is achieved.

Both figures show good agreement between the simulated data and the theoretical curves only for the initial stages of aggregation. In this region, fragmentation effects are still negligible and so, the process corresponds almost to pure DLCA that is known to be well described by the Brownian kernel. For larger times, the stochastic solutions also reach a dynamic equilibrium, even though important discrepancies appear. Here, the theoretical solutions reach the equilibrium earlier and at a smaller weight average cluster size than the simulations. This indicates that the fragmentation rate constants in the aggregation-fragmentation kernel have been overestimated. Hence, it becomes clear that some important effect has not been taken into account in the theoretical description.

In Refs. [11,28], we studied slow irreversible aggregation processes and showed that cluster-cluster collisions that do not lead to bond formation give rise to a situation where the clusters are very close to one another and so, it becomes very likely for them to collide again. In order to consider this effect in the theoretical description, we defined P_{Cij} as the probability for a given pair of clusters to collide again after an unsuccessful collision and used it as a corrective factor for the aggregation kernel. A very similar situation occurs when a cluster breaks into two fragments. Since also here the fragments are very close to one another, it should be equally likely that they collide again and stick together during the next time intervals. Consequently, the probability for this event should be the same as P_{Cij}. Since the overall result of such events is a change in the configuration of the original cluster but not in its mass, an effective cluster fragmentation event occurs only when a bond is broken and the resulting fragments diffuse away. According to the definition of P_{Cij}, this occurs with a probability of $(1-P_{Cij})e_{ij}/\tau$. Consequently, the fragmentation kernel becomes

$$f_{ij}=\frac{e_{ij}(1+\delta_{ij})(1-P_{Cij})}{\tau}=\frac{e_{ij}(1+\delta_{ij})}{\tau\mathcal{N}_{ij}}. \qquad (11)$$

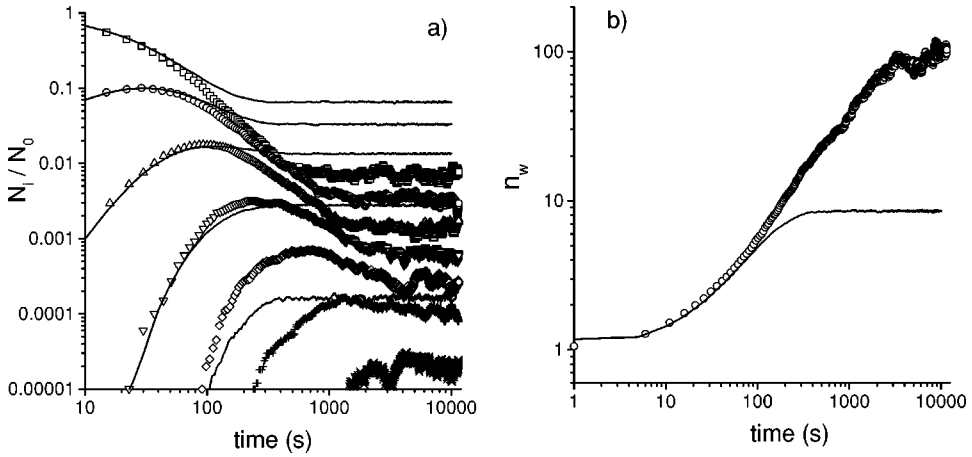

FIG. 4. (a) Time evolution of the cluster-size distribution for $P_r=1\times10^{-5}$. The symbols correspond to the simulated data for monomers up to 200-mers grouped in logarithmically spaced intervals [(□) monomers, (○) 2- and 3-mers, (△) 4- to 8-mers, (▽) 9- to 18-mers, (◇) 19- to 38-mers, (+) 39- to 88-mers, and (×) 89- to 200-mers]. The solid lines represent the stochastic solutions for the aggregation-fragmentation kernel given by Eqs. (4) and (8). (b) Time evolution of the corresponding weight average cluster size n_w.

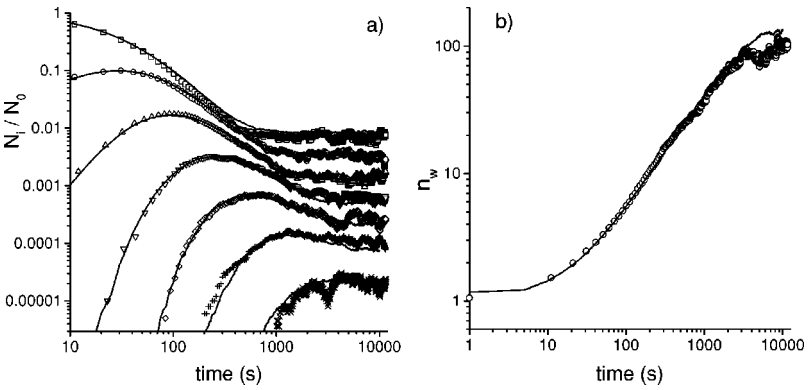

FIG. 5. Time evolution of the cluster-size distribution and weight average cluster size shown in Figs. 4(a) and 4(b). Here, however, the effective aggregation-fragmentation kernel given by Eqs. (4) and (11) was employed for solving the stochastic master equation.

Here, $\mathcal{N}_{ij}$ is the mean number of collisions per encounter for a nonaggregating system. It is related to P_{Cij} by $\mathcal{N}_{ij} = \Sigma_{i=1}^{\infty} i P_{Cij}^{(i-1)}(1-P_{Cij}) = 1/(1-P_{Cij}) = \mathcal{N}_{11}(ij)^b$, where $\mathcal{N}_{11}$ is the mean number of collisions per encounter for monomers and b is a positive constant. The latter parameters were determined in Ref. [11] for similar simulation conditions, obtaining $N_{11}=6.1$ and $b=0.35$.

It should be pointed out that Eq. (11) represents an effective fragmentation kernel, i.e., a kernel that does not consider breakup processes that do not lead to fragment separation. According to Eq. (3), one obtains $\lambda_f=-0.973$ and $\mu_f=-1.493$ for this kernel. This indicates that, although close to the shattering regime, the effective fragmentation kernel still describes a nonshattering process and that dissimilar break up is even more favored. Figures 5(a) and 5(b) compare the time evolution of the simulated cluster-size distribution and weight average cluster size with those obtained theoretically using the effective fragmentation kernel [Eq. (11)]. In this plot, the simulated data are the same than the ones in Figs. 4(a) and 4(b), i.e., they were obtained for a breakup probability of $P_r=1\times10^{-5}$. Now, however, an excellent agreement between the theoretical and simulated data is observed for all times. The considerable fluctuations around the mean values that appear at long aggregation times are due to the relatively poor statistics when only a relatively small number of aggregates remains in the system. Using the effective aggregation-fragmentation kernel, a good agreement was also found for all bond breakup probabilities P_r studied in this paper. As an example, the obtained results for $P_r=5\times10^{-5}$ are shown in Figs. 6(a) and 6(b). As expected, the time necessary for reaching the dynamic equilibrium t^{eq} is shorter than the one corresponding to the smaller fragmentation probability $P_r=1\times10^{-5}$. Furthermore, the equilibrium weight average cluster size n_w^{eq} reached at long times is also considerably smaller. The obtained t^{eq} and n_w^{eq} values are shown in Table I for all bond breakup probabilities. It can be seen that τ, t^{eq}, and n_w^{eq} are strongly correlated. The relatively small number of data points, however, does not allow to determine the analytical relationship that might exist between them. So far, a linear relationship may not be discarded. For $P_r=0$, i.e., the DLCA regime, an average bond lifetime of $\tau=\infty$ was considered and so, the time spent for reaching equilibrium and the corresponding weight average cluster size becomes also infinite.

Since the fragmentation kernel was derived by considering a cluster collection obtained from the asymptotic steady state, the implicitly considered fractal dimension for this kernel was $d_f=2.0$. At early stages, however, fragmentation does not yet play an important role and so, the expected fractal dimension here is approximately 1.75 (DLCA). Consequently, the proposed aggregation-fragmentation kernel should evolve according to this fractal dimension change

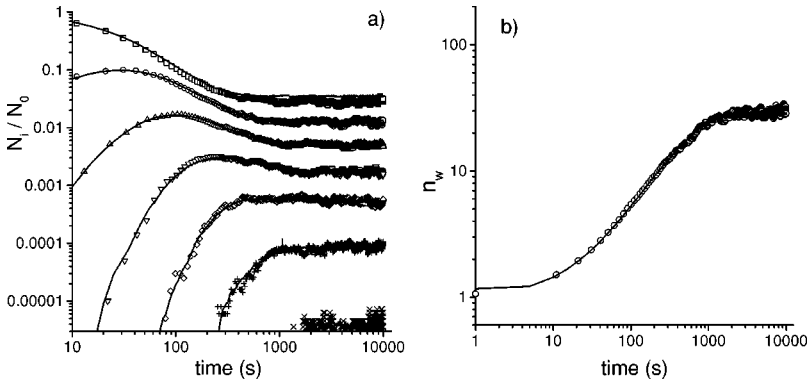

FIG. 6. Time evolution of the cluster-size distribution for $P_r=5\times10^{-5}$. The symbols correspond to the simulated data for monomers up to 200-mers grouped in logarithmically spaced intervals [(□) monomers, (○) 2- and 3-mers, (△) 4- to 8-mers, (▽) 9- to 18-mers, (◇) 19- to 38-mers, (+) 39- to 88-mers, and (×) 89- to 200-mers]. The solid lines represent the stochastic solutions for the effective aggregation-fragmentation kernel given by Eqs. (4) and (11). (b) Time evolution of the corresponding weight average cluster size n_w.

from 1.75 to 2.0. In this study, however, a constant fractal dimension value of 2.0 was considered for the entire aggregation-fragmentation kernel. Hence, some discrepancies may be expected between the calculations and the simulations at the initial stages of the aggregation-fragmentation process. Nevertheless, this is not observed. It may be understood as follows: As mentioned above, at the early stages no significant breakup occurs and hence, the mismatch introduced by the fragmentation kernel should not be detectable. The effect of the different fractal dimension used in the Brownian aggregation kernel is also not observed since its solutions are not very sensitive to d_f changes. According to the literature, DLCA processes can be fitted satisfactorily using even the constant kernel [29].

It should be pointed out that any change in the simulation step length l_0 strongly affects the value of N_{11} and, to a smaller extent, also the value of b. This means that the numerical values of the fitted parameters contained in the aggregation-fragmentation kernel may not be considered as universal and so, it becomes necessary to determine them for any other simulation conditions. The effect of the step length on the simulation of Brownian motion was already studied by Gonzalez [30–33]. He also found a nonuniversal behavior and so, wondered about the correct step length for simulations of aggregation processes. Unfortunately, there is, so far, no answer to this question. In our case, the situation is even worse since we need to introduce an additional separation distance l_s for fragmentation events and again here, the same question arises: How far should the fragments be separated? On one hand, one should keep in mind that Brownian motion is already taken into account by l_0. Hence, l_s should be zero, i.e., the bound is broken but no movement is made until the next step. On the other hand, when an bound is physically broken the corresponding particles have to get out of their respective energetic minimum and hence, some minimum separation becomes necessary. We chose $l_s = a/10$ as a reasonable value. Furthermore, changes in l_s even by a factor of 2 showed to have no important effect on the simulations.

As mentioned above, the effective fragmentation kernel considers only those fragmentation events that give rise to a definitive cluster breakup. The cluster-size distribution obtained from simulations, however, also accounts for the recently produced fragments that may not survive the next simulation step. Depending on the importance of this effect, one expects the equilibrium weight average cluster size n_w^{eq} calculated from the simulated data to be smaller than the analytical solution or not. The fact that there was no significant deviation between the theoretical and the simulated data, indicates that the number of these unstable fragments should be small in comparison with the stable ones. This implies also that the unstable fragments have quite a short average lifetime and so, the time t_c spent between two consecutive collisions of a pair of clusters must be very small. This supports the assumption, $t_c \simeq 0$, used in Refs. [11,28] for deducing an analytical kernel for irreversible aggregation processes.

V. CONCLUSIONS

Starting from the hypothesis of a constant bond breakup probability, it was possible to deduce an analytical kernel for aggregation-fragmentation processes. For this purpose, the fragmentation possibilities of 10^5 different clusters, obtained from computer simulations, were analyzed. The deduced fragmentation kernel was shown to be of nonshattering type. In order to check its validity, aggregation-fragmentation processes were simulated for different average bond lifetimes and the obtained cluster-size distributions were confronted with the corresponding solutions of the reversible master equation. However, important discrepancies were found. These discrepancies could be overcome by introducing the concept of fragmentation effectiveness, i.e., it became necessary to consider as cluster fragmentation only those events where a bond breaks and the obtained fragments are separate enough so that they will not stick again during the following time steps. The fact that the solutions corresponding to the effective aggregation-fragmentation kernel agree so well with the simulated data proves the consistency of the model. At this point, we would like to point out that these results back the assumptions $\mathcal{N}_{ij} = \mathcal{N}_{11}(ij)^b$ and $t_c \simeq 0$ introduced in Ref. [11].

ACKNOWLEDGMENTS

This work was supported by the ''Ministerio de Ciencia y Tecnología [Plan Nacional de Investigación Científica, Desarrollo e Innovación Tecnológica (I+D+I),'' Project MAT 2000-1550-C03-01]. G.O. is grateful for financial support from the *European Union* (Program: αlfa, proposal No. ALR/B7-3011/94.04-6.017.9).

[1] F. Family and D.P. Landau, *Kinetics of Aggregation and Gelation* (North-Holland, Amsterdam, 1984).
[2] H. Sonntag and K. Strenge, *Kinetics and Structure Formation* (Plenum Press, New York, 1987).
[3] R. Hidalgo Álvarez, A. Martín, A. Fernández, D. Bastos, F. Martínez, and F.J. de las Nieves, Adv. Colloid Interface Sci. **67**, 1 (1996).
[4] R.M. Ziff and E.D. McGrady, J. Phys. A **18**, 3027 (1985).
[5] L. Quali and E. Pefferkorn, J. Colloid Interface Sci. **161**, 237 (1993).
[6] M. Thorn, M.L. Broide, and M. Seesselberg, Phys. Rev. E **51**, 4089 (1995).
[7] E. Pefferkorn and S. Stoll, J. Colloid Interface Sci. **138**, 261 (1990).
[8] E. Pefferkorn and J. Widmaier, Colloids Surfaces A. Physicochem. Eng. Aspects **145**, 25 (1998).
[9] F. Elfarissi and E. Pefferkorn, J. Colloid Interface Sci. **221**, 64 (2000).
[10] D.T. Gillespie, J. Phys. Chem. **81**, 2340 (1977).
[11] G. Odriozola, A. Moncho Jordá, A. Schmitt, J. Callejas

Fernández, R. Martínez García, and R. Hidalgo Álvarez, Europhys. Lett. **53**, 797 (2001).
[12] M. Thorn and M. Seesselberg, Phys. Rev. Lett. **72**, 3622 (1994).
[13] P.G.J. van Dongen and M.H. Ernst, J. Stat. Phys. **50**, 295 (1988).
[14] P. Meakin and M.H. Ernst, Phys. Rev. Lett. **60**, 2503 (1988).
[15] E.D. McGrady and R.M. Ziff, Phys. Rev. Lett. **58**, 892 (1987).
[16] M.H. Ernst and P.G.J. van Dongen, Phys. Rev. A **36**, 435 (1987).
[17] M. von Smoluchowski, Phys. Z. **17**, 557 (1916).
[18] M. von Smoluchowski, Z. Phys. Chem. **92**, 129 (1917).
[19] F. Family, P. Meakin, and J.M. Deutch, Phys. Rev. Lett. **57**, 727 (1986).
[20] H. Lichtenfeld, V. Shilov, and L. Knapschinsky, Colloids Surfaces A. Physicochem. Eng. Aspects **142**, 155 (1998).
[21] H. Lichtenfeld, L. Knapschinsky, H. Sonntag, and V. Shilov, Colloids Surfaces A. Physicochem. Eng. Aspects **104**, 313 (1995).
[22] A. Schmitt, G. Odriozola, A. Moncho-Jordá, J. Callejas Fernández, R. Martínez García, and R. Hidalgo Álvarez, Phys. Rev. E **62**, 8335 (2000).
[23] M. Tirado Miranda, A. Schmitt, J. Callejas Fernández, and A. Fernández Barbero, Langmuir **15**, 3437 (1999).
[24] T. Vicsek, *Fractal Growth Phenomena*, 2nd ed. (World Scientific, Singapore, 1992).
[25] M. Kolb, J. Phys. A **19**, L263 (1986).
[26] R. Wessel and R.C. Ball, Phys. Rev. A **45**, 2177 (1992).
[27] R. Wessel and R.C. Ball, J. Phys. A **26**, L159 (1993).
[28] A. Moncho Jordá, G. Odriozola, F. Martínez López, A. Schmitt, and R. Hidalgo Álvarez, Eur. Phys. J. E **5**, 471 (2001).
[29] G. Odriozola, A. Schmitt, J. Callejas Fernández, R. Martínez García, and R. Hidalgo Álvarez, J. Chem. Phys. **111**, 7657 (1999).
[30] A.E. González, Phys. Lett. A **171**, 293 (1992).
[31] A.E. González, Phys. Rev. Lett. **71**, 2248 (1993).
[32] A.E. González, J. Phys. A **26**, 4215 (1993).
[33] A.E. González, Phys. Rev. E **47**, 2923 (1993).